PERGAMON

International Journal of Solids and Structures 40 (2003) 3869–3892

INTERNATIONAL JOURNAL OF SOLIDS and STRUCTURES

www.elsevier.com/locate/ijsolstr

Postbuckling of piezoelectric FGM plates subject to thermo-electro-mechanical loading

K.M. Liew [a,b,*], J. Yang [c], S. Kitipornchai [d]

[a] *Nanyang Centre for Supercomputing and Visualisation, Nanyang Technological University, Nanyang Avenue, Singapore 639798, Singapore*

[b] *School of Mechanical and Production Engineering, Nanyang Technological University, Nanyang Avenue, Singapore 639798, Singapore*

[c] *Department of Civil Engineering, University of Queensland, St. Lucia, Brisbane, Queensland 4072, Australia*

[d] *Department of Building and Construction, City University of Hong Kong, Tat Chee Avenue, Kowloon, Hong Kong*

Received 4 October 2002; received in revised form 15 January 2003

Abstract

In this paper, we examine the postbuckling behavior of functionally graded material FGM rectangular plates that are integrated with surface-bonded piezoelectric actuators and are subjected to the combined action of uniform temperature change, in-plane forces, and constant applied actuator voltage. A Galerkin-differential quadrature iteration algorithm is proposed for solution of the non-linear partial differential governing equations. To account for the transverse shear strains, the Reddy higher-order shear deformation plate theory is employed. The bifurcation-type thermo-mechanical buckling of fully clamped plates, and the postbuckling behavior of plates with more general boundary conditions subject to various thermo-electro-mechanical loads, are discussed in detail. Parametric studies are also undertaken, and show the effects of applied actuator voltage, in-plane forces, volume fraction exponents, temperature change, and the character of boundary conditions on the buckling and postbuckling characteristics of the plates.

Keywords: Buckling; Postbuckling; FGMs; Piezoelectric materials; Hybrid plates; Thermo-electro-mechanical load; Higher-order shear deformation plate theory

1. Introduction

The use of smart materials, as sensors and actuators, for the control of the mechanical behavior of smart structural systems, is becoming more prevalent. Some examples of the smart materials deployed include piezoelectrics, shape memory alloys and rheological-fluids. Here, we aim to investigate the buckling and postbuckling behaviors of piezoelectric functionally graded material (FGM) hybrid plates, a study which has not been previously conducted.

* Corresponding author. Tel.: +65-6790-4076; fax: +65-6793-6763.
E-mail address: mkmliew@ntu.edu.sg (K.M. Liew).

0020-7683/03/$ - see front matter © 2003 Elsevier Science Ltd. All rights reserved.
doi:10.1016/S0020-7683(03)00096-9

FGMs are microscopically inhomogeneous composites that were developed by Japanese scientists in the late 1980s. By smoothly changing the volume fraction of the material constituents, the material properties of FGMs exhibit a continuous variation from one surface to the other, thus eliminating the interface problem that usually takes place in homogeneous composites. The macro-responses of FGM plate structures under thermal and/or mechanical loading have gained increasing attention in recent years, especially from Tanigawa et al. (1991), Praveen and Reddy (1998), Reddy (2000), Shen (2002), Yang and Shen (2002a), and Liew and Liang (2002). However, the investigation of buckling and postbuckling behavior is scarce. Feldman and Aboudi (1997) made the first attempt when they discussed the elastic buckling of uniaxially compressed FGM plates with the volume fractions of the constituents being the function of spatial co-ordinates (x, y, z). Solutions for plates with simply supported and clamped edges were obtained. However, some of the results are questionable because, in most cases, no bifurcational buckling could occur due to the bending–stretching coupling effect in FGM plates. Most recently, Yang and Shen (2002b) investigated the postbuckling behavior of FGM rectangular plates under transverse and in-plane loads by using a semi-analytical DQ-based perturbation technique. In these two analyses, classical plate theory (CPT) was used, and thermal load due to temperature variation was not taken into consideration.

Many studies have reported on the modeling and analysis of smart structures that incorporate surface-bonded or embedded adaptive piezoelectric materials with composite substrates, as reviewed by Chee et al. (1998) and Irschik (2002). In terms of the postbuckling deformation of laminated plates with piezoelectric effects, Oh et al. (2000) presented non-linear finite element formulations for the postbuckling of fully symmetric and partially eccentric piezolaminated composite plates by using layerwise laminated theory. Shen investigated the thermal postbuckling (Shen, 2001a) and thermo-mechanical postbuckling responses (Shen, 2001b) of simply supported, imperfect shear deformable rectangular plates that were covered with piezoelectric actuators. Reddy's higher-order shear deformation plate theory (HSDT) and a mixed Galerkin-perturbation approach were used. As far as the authors are aware, only a few papers in the literature deal with the structural responses of FGM plates with piezoelectric effects (Ootao and Tanigawa, 2000; He et al., 2001, 2002; Liew et al., 2001a, 2002; Ng et al., 2002), and no prior work has been done on the buckling and postbuckling characteristics of piezoelectric FGM hybrid plates.

Hence, this paper is devoted to modeling the buckling and postbuckling behavior of piezoelectric FGM hybrid rectangular plates under the combined action of uniform temperature change, in-plane forces, and constant applied control voltage in the framework of HSDT (Reddy, 1984) by using a semi-analytical one-dimensional differential quadrature (DQ) approximation based iterative approach. Subset problems include the bifurcational buckling of clamped plates due to thermal loads and/or edge compression, thermal postbuckling, compressive postbuckling, and the thermo-mechanical postbuckling of plates with more general boundary conditions. Extensive numerical results of dimensionless critical buckling load and temperature parameters, and the postbuckling equilibrium paths, are presented in tabular and graphical forms respectively.

2. Problem statement

The FGM hybrid rectangular plate under current consideration is defined in a Cartesian co-ordinate system (X, Y, Z), where $X \in [0, a]$, $Y \in [0, b]$ are co-ordinates of a point along the in-plane directions of the plate and Z is the co-ordinate that is perpendicular to the mid-plane and points upwards. The plate is comprised of an FGM substrate of thickness h and piezoelectric films of thickness h_a that are perfectly bonded on its top and bottom surfaces as actuators. The FGM layer is made of a combined ceramic-metal material, the mixing ratio of which is varied continuously and smoothly in the Z direction so that its top surface $(Z = h/2)$ is pure ceramic, while its bottom surface $(Z = -h/2)$ is pure metal. The material distribution is governed by

$$V_c(Z) = \left(\frac{2Z+h}{2h}\right)^n, \quad V_m(Z) = 1 - \left(\frac{2Z+h}{2h}\right)^n \tag{1}$$

where $V(Z)$ is the volume fraction of a material constituent, n is a non-negative volume fraction exponent, and subscripts c and m stand for ceramic and metal. The effective material properties P_{eff}, such as Young's modulus E, Poisson's ratio ν, coefficient of thermal expansion α, can be determined as

$$P_{\text{eff}} = (P_c - P_m)\left(\frac{2Z+h}{2h}\right)^n + P_m \tag{2}$$

Suppose that both the FGM and the piezoelectric material are linear elastic throughout the deformation, and that the plate is initially stress free at T_0 and is then subjected to a uniform temperature variation $\Delta T = T - T_0$, a constant electric field (E_X, E_Y, E_Z), and uniform edge forces $\bar{p}_X$ along X-axis and $\bar{p}_Y$ along Y-axis. The present work aims to reveal the buckling and postbuckling behavior of the plate under the combined action of these thermo-electro-mechanical loads.

3. Theoretical formulations

3.1. Governing equations

Let $\overline{U}$, $\overline{V}$, and $\overline{W}$ be the plate displacements parallel to the co-ordinates (X, Y, Z), let $\overline{\Psi}_X$ and $\overline{\Psi}_Y$ be the mid-plane rotations of transverse normals about the Y and X axes, and let $\overline{U}_0$, $\overline{V}_0$, $\overline{W}_0$ represent the displacements on the mid-plane $(Z = 0)$ of the plate. According to Reddy's HSDT (Reddy, 1984), the displacement field of the plate is assumed to be

$$\overline{U}(X,Y,Z) = \overline{U}_0(X,Y) + Z\overline{\Psi}_X(X,Y) - c_1 Z^3(\overline{\Psi}_X + \overline{W}_{0,X}) \tag{3a}$$

$$\overline{V}(X,Y,Z) = \overline{V}_0(X,Y) + Z\overline{\Psi}_Y(X,Y) - c_1 Z^3(\overline{\Psi}_Y + \overline{W}_{0,Y}) \tag{3b}$$

$$\overline{W}(X,Y,Z) = \overline{W}_0(X,Y) \tag{3c}$$

where $c_1 = 4/3h^2$, and the commas denote partial differentiation with respect to the corresponding co-ordinates. As geometric non-linearity due to moderately large deflection and small rotations is considered in the analysis, the non-linear strains can be derived from the above displacement field and by using von Karman's assumptions as follows

$$\begin{Bmatrix} \varepsilon_X \\ \varepsilon_Y \\ \gamma_{XY} \end{Bmatrix} = \begin{Bmatrix} \varepsilon_X^{(0)} \\ \varepsilon_Y^{(0)} \\ \gamma_{XY}^{(0)} \end{Bmatrix} + Z\begin{Bmatrix} \varepsilon_X^{(1)} \\ \varepsilon_Y^{(1)} \\ \gamma_{XY}^{(1)} \end{Bmatrix} + Z^3\begin{Bmatrix} \varepsilon_X^{(3)} \\ \varepsilon_Y^{(3)} \\ \gamma_{XY}^{(3)} \end{Bmatrix} \tag{4}$$

$$\begin{Bmatrix} \gamma_{YZ} \\ \gamma_{ZX} \end{Bmatrix} = \begin{Bmatrix} \gamma_{YZ}^{(0)} \\ \gamma_{ZX}^{(0)} \end{Bmatrix} + Z^2\begin{Bmatrix} \gamma_{YZ}^{(2)} \\ \gamma_{ZX}^{(2)} \end{Bmatrix} \tag{5}$$

where

$$\{\boldsymbol{\varepsilon}^{(0)}\} = \begin{Bmatrix} \varepsilon_X^{(0)} \\ \varepsilon_Y^{(0)} \\ \gamma_{XY}^{(0)} \end{Bmatrix} = \begin{Bmatrix} \overline{U}_{0,X} + \frac{1}{2}(\overline{W}_{,X})^2 \\ \overline{V}_{0,Y} + \frac{1}{2}(\overline{W}_{,Y})^2 \\ \overline{U}_{0,Y} + \overline{V}_{0,X} + \overline{W}_{,X}\overline{W}_{,Y} \end{Bmatrix}, \quad \{\boldsymbol{\varepsilon}^{(1)}\} = \begin{Bmatrix} \varepsilon_X^{(1)} \\ \varepsilon_Y^{(1)} \\ \gamma_{XY}^{(1)} \end{Bmatrix} = \begin{Bmatrix} \overline{\Psi}_{X,X} \\ \overline{\Psi}_{Y,Y} \\ \overline{\Psi}_{X,Y} + \overline{\Psi}_{Y,X} \end{Bmatrix}$$

$$\{\boldsymbol{\varepsilon}^{(3)}\} = \begin{Bmatrix} \varepsilon_X^{(3)} \\ \varepsilon_Y^{(3)} \\ \gamma_{XY}^{(3)} \end{Bmatrix} = -c_1 \begin{Bmatrix} \overline{\Psi}_{X,X} + \overline{W}_{,XX} \\ \overline{\Psi}_{Y,Y} + \overline{W}_{,YY} \\ \overline{\Psi}_{X,Y} + \overline{\Psi}_{Y,X} + 2\overline{W}_{,XY} \end{Bmatrix}, \quad \{\boldsymbol{\gamma}^{(0)}\} = \begin{Bmatrix} \gamma_{YZ}^{(0)} \\ \gamma_{ZX}^{(0)} \end{Bmatrix} = \begin{Bmatrix} \overline{\Psi}_Y + \overline{W}_{,Y} \\ \overline{\Psi}_X + \overline{W}_{,X} \end{Bmatrix} \tag{6}$$

$$\{\boldsymbol{\gamma}^{(2)}\} = \begin{Bmatrix} \gamma_{YZ}^{(2)} \\ \gamma_{ZX}^{(2)} \end{Bmatrix} = -3c_1 \begin{Bmatrix} \overline{\Psi}_Y + \overline{W}_{,Y} \\ \overline{\Psi}_X + \overline{W}_{,X} \end{Bmatrix}$$

The linear stress–strain relationship for hybrid FGM plates, taking into account the piezoelectric and thermal effects, is given by

$$\begin{Bmatrix} \sigma_X \\ \sigma_Y \\ \tau_{YZ} \\ \tau_{ZX} \\ \tau_{XY} \end{Bmatrix} = \begin{bmatrix} Q_{11} & Q_{12} & 0 & 0 & 0 \\ Q_{12} & Q_{22} & 0 & 0 & 0 \\ 0 & 0 & Q_{44} & 0 & 0 \\ 0 & 0 & 0 & Q_{55} & 0 \\ 0 & 0 & 0 & 0 & Q_{66} \end{bmatrix} \left(\begin{Bmatrix} \varepsilon_X \\ \varepsilon_Y \\ \gamma_{YZ} \\ \gamma_{ZX} \\ \gamma_{XY} \end{Bmatrix} - \begin{Bmatrix} \alpha \\ \alpha \\ 0 \\ 0 \\ 0 \end{Bmatrix} \Delta T \right) - \begin{bmatrix} 0 & 0 & e_{31} \\ 0 & 0 & e_{32} \\ 0 & 0 & 0 \\ 0 & e_{24} & 0 \\ e_{15} & 0 & 0 \end{bmatrix} \begin{Bmatrix} E_X \\ E_Y \\ E_Z \end{Bmatrix} \tag{7}$$

where Q_{ij} $(i,j = 1,2,4,5,6)$ is the elastic stiffness of the FGM layer given by

$$Q_{11} = Q_{22} = \frac{E}{1-v^2}; \quad Q_{12} = \frac{vE}{1-v^2}; \quad Q_{44} = Q_{55} = Q_{66} = \frac{E}{2(1+v)} \tag{8}$$

Piezoelectric stiffness e_{31}, e_{32}, e_{15}, e_{24} can be expressed in terms of the dielectric constants d_{31}, d_{32}, d_{15}, d_{24} and the elastic stiffness Q_{ij}^a $(i,j = 1,2,4,5,6)$ of the piezoelectric actuator layers as

$$e_{31} = (d_{31}Q_{11}^a + d_{32}Q_{12}^a), \quad e_{32} = (d_{31}Q_{12}^a + d_{32}Q_{22}^a), \quad e_{24} = d_{24}Q_{44}^a, \quad e_{15} = d_{15}Q_{55}^a \tag{9}$$

As only transverse electric field component E_Z is dominant in plate type piezoelectric material, it is assumed that

$$[E_X \quad E_Y \quad E_Z]^{\mathrm{T}} = [0 \quad 0 \quad V_{\mathrm{a}}/h_{\mathrm{a}}]^{\mathrm{T}} \tag{10}$$

where V_{a} is the voltage that is applied to the actuators in the thickness direction.

The total stress resultants are defined by a semi-inverse relationship as

$$\begin{Bmatrix} \boldsymbol{\varepsilon}^{(0)} \\ \overline{\mathbf{M}} - \overline{\mathbf{M}}^* \\ \overline{\mathbf{P}} - \overline{\mathbf{P}}^* \end{Bmatrix} = \begin{bmatrix} \mathbf{A}^* & \mathbf{B}^* & \mathbf{E}^* \\ -(\mathbf{B}^*)^{\mathrm{T}} & \mathbf{D}^* & (\mathbf{F}^*)^{\mathrm{T}} \\ -(\mathbf{E}^*)^{\mathrm{T}} & \mathbf{F}^* & \mathbf{H}^* \end{bmatrix} \begin{Bmatrix} \overline{\mathbf{N}} - \overline{\mathbf{N}}^* \\ \boldsymbol{\varepsilon}^{(1)} \\ \boldsymbol{\varepsilon}^{(3)} \end{Bmatrix} \tag{11}$$

$$\begin{Bmatrix} \overline{\mathbf{Q}} \\ \overline{\mathbf{R}} \end{Bmatrix} = \begin{bmatrix} \mathbf{A} & \mathbf{D} \\ \mathbf{D} & \mathbf{F} \end{bmatrix} \begin{Bmatrix} \boldsymbol{\gamma}^{(0)} \\ \boldsymbol{\gamma}^{(2)} \end{Bmatrix} \tag{12}$$

where $\overline{N}^*$, $\overline{M}^*$, $\overline{P}^*$ are the sums of the in-plane forces, moments, and higher-order moments due to the temperature change and electric field: that is,

$$\overline{N}^* = \overline{N}^{\mathrm{T}} + \overline{N}^{\mathrm{E}}, \quad \overline{M}^* = \overline{M}^{\mathrm{T}} + \overline{M}^{\mathrm{E}}, \quad \overline{P}^* = \overline{P}^{\mathrm{T}} + \overline{P}^{\mathrm{E}} \tag{13}$$

Among these, the thermal stress resultants are

$$\begin{bmatrix} \overline{N}_X^{\mathrm{T}} & \overline{M}_X^{\mathrm{T}} & \overline{P}_X^{\mathrm{T}} \\ \overline{N}_Y^{\mathrm{T}} & \overline{M}_Y^{\mathrm{T}} & \overline{P}_Y^{\mathrm{T}} \\ \overline{N}_{XY}^{\mathrm{T}} & \overline{M}_{XY}^{\mathrm{T}} & \overline{P}_{XY}^{\mathrm{T}} \end{bmatrix} = \int_{-h/2}^{h/2} (1, Z, Z^3) \begin{Bmatrix} A_X \\ A_Y \\ A_{XY} \end{Bmatrix} \Delta T \, \mathrm{d}Z = \begin{bmatrix} A_X^{\mathrm{T}} & D_X^{\mathrm{T}} & F_X^{\mathrm{T}} \\ A_Y^{\mathrm{T}} & D_Y^{\mathrm{T}} & F_Y^{\mathrm{T}} \\ A_{XY}^{\mathrm{T}} & D_{XY}^{\mathrm{T}} & F_{XY}^{\mathrm{T}} \end{bmatrix} \Delta T \tag{14}$$

and the electric stress resultants are

$$\begin{bmatrix} \overline{N}_X^{\mathrm{E}} & \overline{M}_X^{\mathrm{E}} & \overline{P}_X^{\mathrm{E}} \\ \overline{N}_Y^{\mathrm{E}} & \overline{M}_Y^{\mathrm{E}} & \overline{P}_Y^{\mathrm{E}} \\ \overline{N}_{XY}^{\mathrm{E}} & \overline{M}_{XY}^{\mathrm{E}} & \overline{P}_{XY}^{\mathrm{E}} \end{bmatrix} = \sum_{k=1}^{N_{\mathrm{a}}} \int_{Z_k}^{Z_{k+1}} (1, Z, Z^3) \begin{Bmatrix} B_X \\ B_Y \\ B_{XY} \end{Bmatrix} E_Z \, \mathrm{d}Z = \begin{bmatrix} A_X^{\mathrm{E}} & D_X^{\mathrm{E}} & F_X^{\mathrm{E}} \\ A_Y^{\mathrm{E}} & D_Y^{\mathrm{E}} & F_Y^{\mathrm{E}} \\ A_{XY}^{\mathrm{E}} & D_{XY}^{\mathrm{E}} & F_{XY}^{\mathrm{E}} \end{bmatrix} E_Z \tag{15}$$

where

$$\begin{Bmatrix} A_X \\ A_Y \\ A_{XY} \end{Bmatrix} = -\begin{Bmatrix} (Q_{11} + Q_{12})\alpha \\ (Q_{11} + Q_{12})\alpha \\ 0 \end{Bmatrix}, \quad \begin{Bmatrix} B_X \\ B_Y \\ B_{XY} \end{Bmatrix} = -\begin{Bmatrix} d_{31}Q_{11}^a + d_{32}Q_{12}^a \\ d_{31}Q_{12}^a + d_{32}Q_{22}^a \\ 0 \end{Bmatrix} \tag{16}$$

The reduced stiffness of the plate A_{ij}^*, B_{ij}^*, D_{ij}^*, E_{ij}^*, F_{ij}^*, H_{ij}^* $(i, j = 1, 2, 6)$ are determined by

$$\mathbf{A}^* = \mathbf{A}^{-1}, \quad \mathbf{B}^* = -\mathbf{A}^{-1}\mathbf{B}, \quad \mathbf{D}^* = \mathbf{D} - \mathbf{B}\mathbf{A}^{-1}\mathbf{B}, \quad \mathbf{E}^* = -\mathbf{A}^{-1}\mathbf{E}, \quad \mathbf{F}^* = \mathbf{F} - \mathbf{E}\mathbf{A}^{-1}\mathbf{B}, \quad \mathbf{H}^* = \mathbf{H} - \mathbf{E}\mathbf{A}^{-1}\mathbf{E} \tag{17}$$

in which only the stiffness elements that are associated with subscripts "16", "26", "61" and "62" are zero, and

$$(A_{ij}, B_{ij}, D_{ij}, E_{ij}, F_{ij}, H_{ij}) = \int_{-h/2}^{h/2} Q_{ij}(1, Z, Z^2, Z^3, Z^4, Z^6) \, \mathrm{d}Z + \sum_{k=1}^{N_{\mathrm{a}}} \int_{Z_k}^{Z_{k+1}} Q_{ij}^a(1, Z, Z^2, Z^3, Z^4, Z^6) \, \mathrm{d}Z \quad (i, j = 1, 2, 6) \tag{18}$$

$$(A_{ij}, D_{ij}, F_{ij}) = \int_{-h/2}^{h/2} Q_{ij}(1, Z^2, Z^4) \, \mathrm{d}Z + \sum_{k=1}^{N_{\mathrm{a}}} \int_{Z_k}^{Z_{k+1}} Q_{ij}^a(1, Z^2, Z^4) \, \mathrm{d}Z \quad (i, j = 4, 5) \tag{19}$$

Here N_{a} is the number of actuator layers.

Let $\overline{F}(X, Y)$ be the stress function that is related to stress resultants by $\overline{N}_X = \overline{F}_{,YY}$, $\overline{N}_Y = \overline{F}_{,XX}$, $\overline{N}_{XY} = -\overline{F}_{,XY}$. We can derive the HSDT-based non-linear equilibrium equations of hybrid FGM plates as follows:

$$\overline{Q}_{X,X} + \overline{Q}_{Y,Y} - 3c_1(\overline{R}_{X,X} + \overline{R}_{Y,Y}) + c_1(\overline{P}_{X,XX} + 2\overline{P}_{XY,XY} + \overline{P}_{Y,YY}) = \widetilde{L}(\overline{W}, \overline{F}) \tag{20}$$

$$\overline{M}_{X,X} + \overline{M}_{XY,Y} - \overline{Q}_X + 3c_1\overline{R}_X - c_1(\overline{P}_{X,X} + \overline{P}_{XY,Y}) = 0 \tag{21}$$

$$\overline{M}_{XY,X} + \overline{M}_{Y,Y} - \overline{Q}_Y + 3c_1\overline{R}_Y - c_1(\overline{P}_{XY,X} + \overline{P}_{Y,Y}) = 0 \tag{22}$$

The compatibility condition states that

$$\varepsilon_{X,YY} + \varepsilon_{Y,XX} - \gamma_{XY,XY} = (\overline{W}_{,XY})^2 - \overline{W}_{,XX}\overline{W}_{,YY} \tag{23}$$

where the non-linear partial differential operator $\widetilde{L}(\ ) = (\ )_{,XX}(\ )_{,YY} - 2(\ )_{,XY}(\ )_{,XY} + (\ )_{,YY}(\ )_{,XX}$.

3.2. Dimensionless governing equations

By putting Eqs. (11) and (12) into equilibrium equations (20)–(22), applying Eqs. (4) and (11) to compatibility equation (23), and introducing the following dimensionless quantities,

$$
\begin{aligned}
&x = X/a, \quad y = Y/b, \quad \beta = a/b, \quad \Delta = (D_{11}^* D_{22}^* A_{11}^* A_{22}^*)^{1/4}, \quad \lambda_T = 1000\alpha_c \Delta T, \quad W = \overline{W}/\Delta \\
&F = \overline{F}/(D_{11}^* D_{22}^*)^{1/2}, \quad (\Psi_x, \Psi_y) = (\overline{\Psi}_X, \overline{\Psi}_Y)a/\Delta, \quad (\delta_x, \delta_y) = (\bar{\delta}_X/a, \bar{\delta}_Y/b)b^2/\Delta^2 \\
&(\lambda_x, \lambda_y) = (\bar{p}_X b^2, \bar{p}_Y a^2)/(D_{11}^* D_{22}^*)^{1/2}, \quad (N_x^*, N_y^*, N_{xy}^*) = (\overline{N}_X^*, \overline{N}_Y^*, \overline{N}_{XY}^*)a^2/(D_{11}^* D_{22}^*)^{1/2} \\
&(M_x, M_y, M_{xy}, M_x^*, M_y^*, M_{xy}^*) = (\overline{M}_X, \overline{M}_Y, \overline{M}_{XY}, \overline{M}_X^*, \overline{M}_Y^*, \overline{M}_{XY}^*)a^2/D_{11}^* \Delta \\
&(P_x, P_y, P_{xy}, P_x^*, P_y^*, P_{xy}^*) = c_1(\overline{P}_X, \overline{P}_Y, \overline{P}_{XY}, \overline{P}_X^*, \overline{P}_Y^*, \overline{P}_{XY}^*)a^2/D_{11}^* \Delta
\end{aligned} \tag{24}
$$

where $\bar{\delta}_X$, $\bar{\delta}_Y$ imply the in-plane displacements in the X-axis and the Y-axis, and the non-linear governing Eqs. (20)–(23) can be transformed into dimensionless form as

$$L_{11}(W) - L_{12}(\Psi_x) - L_{13}(\Psi_y) + \gamma_{14}L_{14}(F) - L_{15}(N^*) - L_{16}(M^*) = \gamma_{14}\beta^2 L(W, F) \tag{25}$$

$$L_{21}(F) + \gamma_{24}L_{22}(\Psi_x) + \gamma_{24}L_{23}(\Psi_y) - \gamma_{24}L_{24}(W) - L_{25}(N^*) = -\tfrac{1}{2}\gamma_{24}\beta^2 L(W, W) \tag{26}$$

$$L_{31}(W) + L_{32}(\Psi_x) - L_{33}(\Psi_y) + \gamma_{14}L_{34}(F) - L_{35}(N^*) - L_{36}(S^*) = 0 \tag{27}$$

$$L_{41}(W) - L_{42}(\Psi_x) + L_{43}(\Psi_y) + \gamma_{14}L_{44}(F) - L_{45}(N^*) - L_{46}(S^*) = 0 \tag{28}$$

where $S^* = M^* - c_1 P^*$, $L(\ ) = (\ )_{,xx}(\ )_{,yy} - 2(\ )_{,xy}(\ )_{,xy} + (\ )_{,yy}(\ )_{,xx}$. The linear partial differential operators are the same as those that are given by Yang and Shen (2002a), with the exception of those that are associated with thermal and piezoelectric effects, as follows

$$
\begin{aligned}
&L_{15}(N^*) = [\gamma_{711}N_x^* + \gamma_{721}N_y^*]_{,xx} + 2\beta\gamma_{733}N_{xy,xy}^* + \beta^2[\gamma_{712}N_x^* + \gamma_{722}N_y^*]_{,yy} \\
&L_{16}(M^*) = M_{x,xx}^* + 2\beta M_{xy,xy}^* + \beta^2 M_{y,yy}^* \\
&L_{25}(N^*) = [\gamma_{612}N_x^* + N_y^*]_{,xx} - \beta\gamma_{633}N_{xy,xy}^* + \beta^2[\gamma_{611}N_x^* + \gamma_{612}N_y^*]_{,yy} \\
&L_{35}(N^*) = [\gamma_{511}N_x^* + \gamma_{512}N_y^*]_{,x} + \beta\gamma_{516}N_{xy,y}^*, \quad L_{36}(S^*) = S_{x,x}^* + \beta S_{xy,y}^* \\
&L_{45}(N^*) = \gamma_{516}N_{xy,x}^* + \beta[\gamma_{517}N_x^* + \gamma_{518}N_y^*]_{,y}, \quad L_{46}(S^*) = S_{xy,x}^* + \beta S_{y,y}^*
\end{aligned} \tag{29}
$$

Obviously, these terms will vanish when, in particular, the temperature field and the electric field are uniform through the plate domain, or vary in the Z-direction only.

The non-dimensionalized moments and their higher-order counterparts are of the form

$$
\begin{aligned}
M_x = &-\gamma_{14}(\gamma_{711}\beta^2 F_{,yy} + \gamma_{721}F_{,xx}) + \gamma_{M10}\Psi_{x,x} + \gamma_{M12}\beta\Psi_{y,y} - (\gamma_{M13}W_{,xx} + \gamma_{M14}\beta W_{,yy}) \\
&+ [\gamma_{14}(\gamma_{711}\gamma_{T1} + \gamma_{721}\gamma_{T2}) + \gamma_{T4}]\lambda_T + [\gamma_{14}(\gamma_{711}\gamma_{E1} + \gamma_{721}\gamma_{E2}) + \gamma_{E4}]E_Z
\end{aligned} \tag{30a}
$$

$$
\begin{aligned}
M_y = &-\gamma_{14}(\gamma_{712}\beta^2 F_{,yy} + \gamma_{722}F_{,xx}) + \gamma_{M20}\Psi_{x,x} + \gamma_{M22}\beta\Psi_{y,y} - (\gamma_{M23}W_{,xx} + \gamma_{M24}\beta W_{,yy}) \\
&+ [\gamma_{14}(\gamma_{712}\gamma_{T1} + \gamma_{722}\gamma_{T2}) + \gamma_{T5}]\lambda_T + [\gamma_{14}(\gamma_{712}\gamma_{E1} + \gamma_{722}\gamma_{E2}) + \gamma_{E5}]E_Z
\end{aligned} \tag{30b}
$$

$$M_{xy} = \gamma_{14}\gamma_{733}\beta F_{,xy} + \gamma_{M31}(\Psi_{y,x} + \beta\Psi_{x,y}) - 2\gamma_{M35}\beta W_{,xy} \tag{30c}$$

$$
\begin{aligned}
P_x = &-\gamma_{14}(\gamma_{P18}\beta^2 F_{,yy} + \gamma_{P16}F_{,xx}) + \gamma_{P10}\Psi_{x,x} + \gamma_{P12}\beta\Psi_{y,y} - (\gamma_{P13}W_{,xx} + \gamma_{P14}\beta W_{,yy}) \\
&+ [\gamma_{14}(\gamma_{P18}\gamma_{T1} + \gamma_{P16}\gamma_{T2}) + \gamma_{T7}]\lambda_T + [\gamma_{14}(\gamma_{P18}\gamma_{E1} + \gamma_{P16}\gamma_{E2}) + \gamma_{E7}]E_Z
\end{aligned} \tag{31a}
$$

$$
\begin{aligned}
P_y = &-\gamma_{14}(\gamma_{P28}\beta^2 F_{,yy} + \gamma_{P26}F_{,xx}) + \gamma_{P20}\Psi_{x,x} + \gamma_{P22}\beta\Psi_{y,y} - (\gamma_{P23}W_{,xx} + \gamma_{P24}\beta W_{,yy}) \\
&+ [\gamma_{14}(\gamma_{P28}\gamma_{T1} + \gamma_{P26}\gamma_{T2}) + \gamma_{T8}]\lambda_T + [\gamma_{14}(\gamma_{P28}\gamma_{E1} + \gamma_{P26}\gamma_{E2}) + \gamma_{E8}]E_Z
\end{aligned} \tag{31b}
$$

$$P_{xy} = \gamma_{14}\gamma_{P37}\beta F_{,xy} + \gamma_{P31}(\Psi_{y,x} + \beta\Psi_{x,y}) - 2\gamma_{P35}\beta W_{,xy} \tag{31c}$$

The out-of-plane boundary conditions for simply supported (S), clamped (C), and free (F) edges are

$$\text{S:}\quad W = \Psi_s = M_n = P_n = 0 \tag{32}$$

$$\text{C:}\quad W = \Psi_s = \Psi_n = W_{,n} = 0 \tag{33}$$

$$\text{F:}\quad Q_n^* = M_{ns}^* = M_n = P_n = 0 \tag{34}$$

Depending upon the in-plane supporting characteristics, two types of in-plane constraints, one that is termed "movable", where in-plane expansion/contraction may occur, and another that is termed "immovable", where no in-plane expansion/contraction is allowed, will also be considered. However, in both cases, the tangential motion parallel to the edges is unconstrained. This requires that

$$F_{,ns} = 0, \quad F_{,ss} + \lambda_n^* = 0 \quad \text{(for movable edges)} \tag{35}$$

$$F_{,ns} = 0, \quad \delta_n = 0 \quad \text{(for immovable edges)} \tag{36}$$

Subscripts n and s refer to the normal and tangential directions of the plate edge. M_{ns}^* and Q_n^* are the dimensionless generalized moment and transverse shear force, which are given by

$$M_{xy}^* = \gamma_{m11}\beta W_{,xy} + \gamma_{14}\gamma_{m21}\beta F_{,xy} + \gamma_{m31}(\beta\Psi_{x,y} + \Psi_{y,x}) \tag{37}$$

$$\begin{aligned} Q_x^* = {} & -(\gamma_{Q10}W_{,xxx} + \gamma_{Q12}\beta^2 W_{,xyy} - \gamma_{31}W_{,x}) - \gamma_{14}(\gamma_{Q20}F_{,xxx} + \gamma_{Q22}\beta^2 F_{,xyy}) + \gamma_{31}\Psi_x \\ & + \gamma_{Q30}\Psi_{x,xx} + \gamma_{Q32}\beta^2\Psi_{x,yy} + \gamma_{Q34}\beta\Psi_{y,xy} \end{aligned} \tag{38}$$

In general, the immovable condition cannot be satisfied at every arbitrary point on the corresponding edge, and is therefore fulfilled in a weak form as

$$\delta_x = -(a_x + a_x^{\mathrm{T}}\lambda_T + a_x^{\mathrm{E}}E_Z)/\gamma_{24}\beta^2 = 0 \quad \text{at } x = 0, 1 \tag{39a}$$

$$\delta_y = -(b_y + b_y^{\mathrm{T}}\lambda_T + b_y^{\mathrm{E}}E_Z)/\gamma_{24}\beta^2 = 0 \quad \text{at } y = 0, 1 \tag{39b}$$

where

$$\begin{aligned} a_x &= \int_0^1\int_0^1 \left\{[\gamma_{24}^2\beta^2 F_{,yy} - \gamma_5 F_{,xx} + \gamma_{24}(\gamma_{511}\Psi_{x,x} + \gamma_{233}\beta\Psi_{y,y}) - \gamma_{24}(\gamma_{p18}W_{,xx} + \gamma_{p28}\beta^2 W_{,yy})] - \frac{1}{2}\gamma_{24}(W_{,x})^2\right\}\mathrm{d}x\,\mathrm{d}y \\ b_y &= \int_0^1\int_0^1 \left\{[F_{,xx} - \gamma_5\beta^2 F_{,yy} + \gamma_{24}(\gamma_{512}\Psi_{x,x} + \gamma_{518}\beta\Psi_{y,y}) - \gamma_{24}(\gamma_{p16}W_{,xx} + \gamma_{p26}\beta^2 W_{,yy})] - \frac{1}{2}\gamma_{24}\beta^2(W_{,y})^2\right\}\mathrm{d}y\,\mathrm{d}x \\ a_x^{\mathrm{T}} &= -\int_0^1\int_0^1 (\gamma_{24}^2\gamma_{T1} - \gamma_5\gamma_{T2})\,\mathrm{d}x\,\mathrm{d}y, \quad b_y^{\mathrm{T}} = -\int_0^1\int_0^1 (\gamma_{T2} - \gamma_5\gamma_{T1})\,\mathrm{d}x\,\mathrm{d}y \\ a_x^{\mathrm{E}} &= -\int_0^1\int_0^1 (\gamma_{24}^2\gamma_{E1} - \gamma_5\gamma_{E2})\,\mathrm{d}x\,\mathrm{d}y, \quad b_y^{\mathrm{E}} = -\int_0^1\int_0^1 (\gamma_{E2} - \gamma_5\gamma_{E1})\,\mathrm{d}x\,\mathrm{d}y \end{aligned} \tag{40}$$

To include the uniform membrane stress state in the plate, the stress function is expressed as

$$F = -\tfrac{1}{2}(y^2\lambda_x^* + x^2\lambda_y^*) + f(x, y) \tag{41}$$

where λ_x^* and λ_y^* are combinations of the applied in-plane forces (λ_x, λ_y) and the reactions of immovable constraints, and can be determined according to different in-plane boundary conditions by:

(a) when the plate is immovable at four edges

$$\lambda_x^* = [s_{12}b_y - s_{22}a_x + (s_{12}b_y^{\mathrm{T}} - s_{22}a_x^{\mathrm{T}})\lambda_T + (s_{12}b_y^{\mathrm{E}} - s_{22}a_x^{\mathrm{E}})E_z]/(s_{12}^2 - s_{11}s_{22}) \tag{42a}$$

$$\lambda_y^* = [s_{12}a_x - s_{11}b_y + (s_{12}a_x^{\mathrm{T}} - s_{11}b_y^{\mathrm{T}})\lambda_T + (s_{12}a_x^{\mathrm{E}} - s_{11}b_y^{\mathrm{E}})E_z]/(s_{12}^2 - s_{11}s_{22}) \tag{42b}$$

(b) when the plate is movable at $x = 0, 1$ and immovable at $y = 0, 1$

$$\lambda_x^* = \lambda_x, \quad \lambda_y^* = [b_y + b_y^{\mathrm{T}}\lambda_T + b_y^{\mathrm{E}}E_z - s_{12}\lambda_x]/s_{22} \tag{43a,b}$$

(c) when the plate is immovable at $x = 0, 1$ and movable at $y = 0, 1$

$$\lambda_x^* = [a_x + a_x^{\mathrm{T}}\lambda_T + a_x^{\mathrm{E}}E_z - s_{12}\lambda_y]/s_{11}, \quad \lambda_y^* = \lambda_y \tag{44a,b}$$

(d) when the plate is movable at all edges

$$\lambda_x^* = \lambda_x, \quad \lambda_y^* = \lambda_y \tag{45a,b}$$

where $s_{11} = \gamma_{24}^2/\gamma_{14}$, $s_{12} = \gamma_{612}/\gamma_{14}$, $s_{22} = 1/\gamma_{14}$.

Dimensionless quantities of γ_{ij} and γ_{ijk} are listed in Appendix A.

4. Semi-analytical formulations

A semi-analytical DQ-based iteration process is employed to determine the postbuckling response of the plate. The basic idea is to convert the non-linear partial differential governing Eqs. (25)–(28) and the associated boundary conditions into a set of ordinary differential equations through the DQ approximation in x-axis, and then apply the Galerkin procedure to establish a non-linear algebraic equation system, from which the postbuckling path can be determined by an iterative scheme.

4.1. Solution methodology

As shown in Fig. 1, the plate domain is in the first place discretized along the x-axis by a number of nodal lines parallel to the y-axis, among which $x_2 = 0.0001$ and $x_{N-1} = 0.9999$ are arranged to be quite close to $x_1 = 0$ and $x_N = 1$ to impose the six boundary conditions at each of the two edges ($x = 0, 1$). The other nodal lines are located according to the cosine spacing pattern as

$$x_i = \frac{1}{2}\left[1 - \cos\frac{\pi(i-2)}{N-3}\right] \tag{46}$$

where N is the total number of nodal lines. Designating the unknown function values at an arbitrary sampling nodal line $x = x_i$ as

$$W_i = W(x_i, y), \quad f_i = f(x_i, y), \quad \Psi_{xi} = \Psi_x(x_i, y), \quad \Psi_{yi} = \Psi_y(x_i, y) \;\; i = 1, \ldots, N \tag{47}$$

and applying the DQ rule to the dimensionless partial differential governing equations (25)–(28), yields

$$L_{11}^i(W) - L_{12}^i(\Psi_x) - L_{13}^i(\Psi_y) + \gamma_{14}L_{14}^i(f) = \gamma_{14}\beta^2 L^i(W, f) \tag{48}$$

$$L_{21}^i(f) + \gamma_{24}L_{22}^i(\Psi_x) + \gamma_{24}L_{23}^i(\Psi_y) - \gamma_{24}L_{24}^i(W) = -\tfrac{1}{2}\gamma_{24}\beta^2 L^i(W, W) \tag{49}$$

$$L_{31}^i(W) + L_{32}^i(\Psi_x) - L_{33}^i(\Psi_y) + \gamma_{14}L_{34}^i(f) = 0 \tag{50}$$

$$L_{41}^i(W) - L_{42}^i(\Psi_x) + L_{43}^i(\Psi_y) + \gamma_{14}L_{44}^i(f) = 0 \tag{51}$$

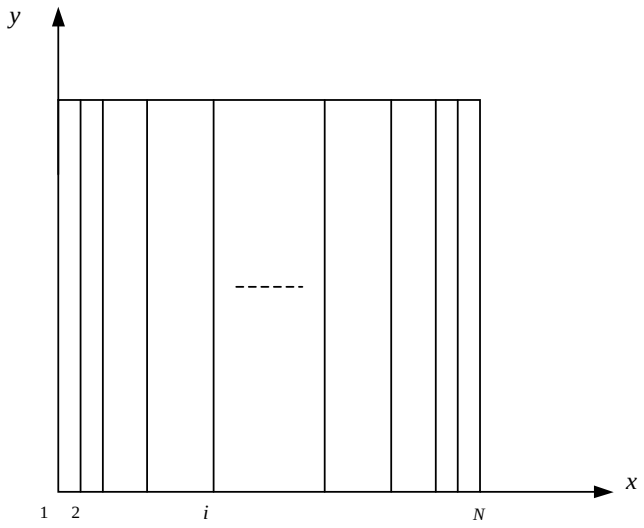

Fig. 1. Nodal line system in a rectangular plate domain.

where the discretized differential operators are

$$L_{11}^{i}(W) = \gamma_{110}\sum_{j=1}^{N} C_{ij}^{(4)} W_j + 2\gamma_{112}\beta^2 \sum_{j=1}^{N} C_{ij}^{(2)} W_{j,yy} + \gamma_{114}\beta^4 W_{i,yyyy} + \gamma_{14}\beta^2 \left(\lambda_x^* \sum_{j=1}^{N} C_{ij}^{(2)} W_j + \lambda_y^* W_{i,yy} \right)$$

$$L_{12}^{i}(\Psi_x) = \left(\gamma_{120}\sum_{j=1}^{N} C_{ij}^{(3)} \Psi_{xj} + \gamma_{122}\beta^2 \sum_{j=1}^{N} C_{ij}^{(1)} \Psi_{xj,yy} \right)$$

$$L_{13}^{i}(\Psi_y) = \beta \left(\gamma_{131}\sum_{j=1}^{N} C_{ij}^{(2)} \Psi_{yj,y} + \gamma_{133}\beta^2 \Psi_{yi,yyy} \right)$$

$$L_{14}^{i}(f) = \left(\gamma_{140}\sum_{j=1}^{N} C_{ij}^{(4)} f_j + \gamma_{142}\beta^2 \sum_{j=1}^{N} C_{ij}^{(2)} f_{j,yy} + \gamma_{144}\beta^4 f_{i,yyyy} \right)$$

$$L^{i}(W,f) = \left(f_{i,yy}\sum_{j=1}^{N} C_{ij}^{(2)} W_j - 2\sum_{j=1}^{N} C_{ij}^{(1)} W_{j,y} \sum_{k=1}^{N} C_{ik}^{(1)} f_{k,y} + W_{i,yy} \sum_{j=1}^{N} C_{ij}^{(2)} f_j \right)$$

$$L_{21}^{i}(f) = \sum_{j=1}^{N} C_{ij}^{(4)} f_j + \gamma_{212}\beta^2 \sum_{j=1}^{N} C_{ij}^{(2)} f_{j,yy} + \gamma_{24}^2 \beta^4 f_{i,yyyy}$$

$$L_{22}^{i}(\Psi_x) = \left(\gamma_{220}\sum_{j=1}^{N} C_{ij}^{(3)} \Psi_{xj} + \gamma_{222}\beta^2 \sum_{j=1}^{N} C_{ij}^{(1)} \Psi_{xj,yy} \right)$$

$$L_{23}^{i}(\Psi_y) = \left(\gamma_{231}\sum_{j=1}^{N} C_{ij}^{(2)} \Psi_{yj,y} + \gamma_{233}\beta^2 \Psi_{yi,yyy} \right)$$

$$L_{24}^{i}(W) = \left(\gamma_{240}\sum_{j=1}^{N} C_{ij}^{(4)} W_j + \gamma_{242}\beta^2 \sum_{j=1}^{N} C_{ij}^{(2)} W_{j,yy} + \gamma_{244}\beta^4 W_{i,yyyy} \right)$$

$$L^i(W,W) = \left(W_{i,yy} \sum_{j=1}^{N} C_{ij}^{(2)} W_j - 2 \sum_{j=1}^{N} C_{ij}^{(1)} W_{j,y} \sum_{k=1}^{N} C_{ik}^{(1)} W_{k,y} + W_{i,yy} \sum_{j=1}^{N} C_{ij}^{(2)} W_j \right)$$

$$L_{31}^i(W) = \gamma_{31} \sum_{j=1}^{N} C_{ij}^{(1)} W_j + \gamma_{310} \sum_{j=1}^{N} C_{ij}^{(3)} W_j + \gamma_{312} \beta^2 \sum_{j=1}^{N} C_{ij}^{(1)} W_{j,yy}$$

$$L_{32}^i(\Psi_x) = \left(\gamma_{31} \Psi_{xi} - \gamma_{320} \sum_{j=1}^{N} C_{ij}^{(2)} \Psi_{xj} - \gamma_{322} \beta^2 \Psi_{xi,yy} \right), \quad L_{33}^i(\Psi_y) = \gamma_{331} \beta \sum_{j=1}^{N} C_{ij}^{(1)} \Psi_{yj,y}$$

$$L_{34}^i(f) = \left(\gamma_{220} \sum_{j=1}^{N} C_{ij}^{(3)} f_j + \gamma_{222} \beta^2 \sum_{j=1}^{N} C_{ij}^{(1)} f_{j,yy} \right)$$

$$L_{41}^i(W) = \gamma_{41} \beta W_{i,y} + \gamma_{411} \beta \sum_{j=1}^{N} C_{ij}^{(2)} W_{j,y} + \gamma_{413} \beta^3 W_{j,yyy}, \quad L_{42}^i(\Psi_x) = \gamma_{331} \beta \sum_{j=1}^{N} C_{ij}^{(1)} \Psi_{xj}$$

$$L_{43}^i(\Psi_y) = \left(\gamma_{41} \Psi_{yi} - \gamma_{430} \sum_{j=1}^{N} C_{ij}^{(2)} \Psi_{yj} - \gamma_{432} \beta^2 \Psi_{yi,yy} \right),$$

$$L_{44}^i(f) = \beta \left(\gamma_{231} \sum_{j=1}^{N} C_{ij}^{(2)} f_{j,y} + \gamma_{233} \beta^2 f_{i,yyy} \right) \quad i = 2, 3, N-2, N-1 \tag{52}$$

Here, $C_{ij}^{(k)}$ is the weighting coefficient for the kth partial derivative of a unknown function with respect to x, and can be determined from the recursive formulae that are given by, for example, Bert and Malik (1996) and Liew et al. (1996). After incorporating the associated boundary conditions that are being discretized in the same way, we obtain a system of $4N$ ordinary differential equations in terms of W_i, f_i, Ψ_{xi}, and Ψ_{yi}.

At each nodal line, W_i, f_i, Ψ_{xi}, and Ψ_{yi} are expanded in series form as

$$\begin{Bmatrix} W_i \\ f_i \\ \Psi_{xi} \\ \Psi_{yi} \end{Bmatrix} = \sum_{m=1}^{M} \begin{bmatrix} a_{im} & 0 & 0 & 0 \\ 0 & b_{im} & 0 & 0 \\ 0 & 0 & c_{im} & 0 \\ 0 & 0 & 0 & d_{im} \end{bmatrix} \begin{Bmatrix} W_{im}(y) \\ f_{im}(y) \\ \Psi_{xim}(y) \\ \Psi_{yim}(y) \end{Bmatrix} \tag{53}$$

where M is the truncated number of the series expansions, and a_{im}, b_{im}, c_{im}, d_{im} are constants to be determined.

Solutions are sought for plates that are clamped at $y = 0, 1$, and free, simply supported, or clamped at $x = 0, 1$. To this end, $W_{im}(y)$, $f_{im}(y)$, $\Psi_{xim}(y)$, and $\Psi_{yim}(y)$ are chosen to satisfy the clamped boundary conditions and take the form of

$$W_{im}(y) = \sin \alpha_m y - \sinh \alpha_m y - \xi_m (\cos \alpha_m y - \cosh \alpha_m y) \tag{54a}$$

$$f_{im}(y) = \sin \alpha_m y - \sinh \alpha_m y - \xi_m (\cos \alpha_m y - \cosh \alpha_m y) \tag{54b}$$

$$\Psi_{xim}(y) = \sin(m\pi y); \quad \Psi_{yim}(y) = \sin(m\pi y) \tag{54c,d}$$

where $\xi_m = (\sin \alpha_m - \sinh \alpha_m)/(\cos \alpha_m - \cosh \alpha_m)$, $\alpha_m = (2m+1)\pi/2$.

Putting Eqs. (53) and (54) into the $4N$ ordinary differential equations, and then applying the Galerkin procedure, gives a non-linear algebraic system that governs the postbuckling behavior of the plate under thermo-electro-mechanical loads as

$$([K_0] + \lambda[K_\lambda] + \lambda_T[K_T] + [K_{\mathrm{NL}}(\Phi)])_{4NM \times 4NM} \{\Phi\}_{4NM \times 1} = \{R\}_{4NM \times 1} \tag{55}$$

where $\{\Phi\}$ implies an unknown vector that is composed of a_{im}, b_{im}, c_{im}, d_{im} ($i = 1, \ldots, N$; $m = 1, \ldots, M$), $\{R\}$ stands for the thermo-electro-mechanical load vector, $[K_0]$ is the constant coefficient matrix, $[K_\lambda]$ and $[K_T]$ are coefficient matrices that are associated with applied in-plane force parameter λ ($\lambda_x = s_x\lambda$, $\lambda_y = s_y\lambda$) and temperature parameter λ_T, $[K_{\mathrm{NL}}]$ is a non-linear matrix that is dependent on $\{\Phi\}$, and s_x and s_y are the proportion ratios for applied in-plane forces.

It should be pointed out that the above solution procedure is also valid for isotropic plates that are simply supported at $y = 0, 1$, but the functions $W_{im}(y)$, $f_{im}(y)$, $\Psi_{xim}(y)$, and $\Psi_{yim}(y)$ should be replaced by

$$W_{im}(y) = \sin(m\pi y) \tag{56a}$$

$$f_{im}(y) = \sin\alpha_m y - \sinh\alpha_m y - \xi_m(\cos\alpha_m y - \cosh\alpha_m y) \tag{56b}$$

$$\Psi_{xim}(y) = \sin(m\pi y); \quad \Psi_{yim}(y) = \cos(m\pi y) \tag{56c,d}$$

4.2. Subset problems

4.2.1. Bifurcation buckling of piezoelectric FGM hybrid plates

Due to the presence of bending–stretching coupling elements in reduced stiffness matrices (17), even minimal in-plane action can give rise to deflections and bending moments in piezoelectric FGM hybrid plates. Therefore, bifurcation-type buckling will not occur, except when the plate is fully clamped. This is because the bending moments that are generated by thermo-electric-mechanical loads can be neutralized by the support reacting moments that are produced by the four clamped edges, and the plate can remain flat before buckling (Leissa, 1986; Qatu and Leissa, 1993). As another special case, isotropic plates, which are free from the bending–stretching coupling effect, are also capable of bifurcation-type buckling.

For clamped piezoelectric FGM hybrid plates, the critical buckling load parameter can be found by solving the following eigenvalue equation

$$([K_0] + \lambda_{\mathrm{cr}}[K_\lambda])_{4NM\times 4NM}\{\Phi\}_{4NM\times 1} = \{0\}_{4NM\times 1} \tag{57}$$

and the critical buckling temperature parameter can be determined from

$$([K_0] + \lambda_{T\mathrm{cr}}[K_T])_{4NM\times 4NM}\{\Phi\}_{4NM\times 1} = \{0\}_{4NM\times 1} \tag{58}$$

The buckling load for a thermally prestressed clamped plate is given by

$$([K_0] + \lambda_T[K_T] + \lambda_{\mathrm{cr}}[K_\lambda])_{4NM\times 4NM}\{\Phi\}_{4NM\times 1} = \{0\}_{4NM\times 1} \tag{59}$$

and the buckling temperature for an initially stressed clamped plate is defined by

$$([K_0] + \lambda[K_\lambda] + \lambda_{T\mathrm{cr}}[K_T])_{4NM\times 4NM}\{\Phi\}_{4NM\times 1} = \{0\}_{4NM\times 1} \tag{60}$$

The lowest eignvalues λ_{cr}, $\lambda_{T\mathrm{cr}}$ denote the critical buckling load parameter and the critical buckling temperature parameter. Note that $\lambda_T < \lambda^0_{T\mathrm{cr}}$ in Eq. (59) and $\lambda < \lambda^0_{\mathrm{cr}}$ in Eq. (60) where λ^0_{cr} is solved from Eq. (57) and $\lambda^0_{T\mathrm{cr}}$ is solved from Eq. (58).

4.2.2. Postbuckling response of piezoelectric FGM hybrid plates

After buckling, the postbuckling equilibrium path of the plate can be traced by solving the non-linear equilibrium equation (55) with an iterative scheme. In this paper, compressive postbuckling ($\lambda_T = 0$), thermal postbuckling ($\lambda = 0$), and thermo-mechanical postbuckling (either λ_T or λ is given) are included as subset problems.

For isotropic or clamped piezoelectric FGM hybrid plates that exhibit bifurcation instability, the right-hand side vector in Eq. (55) becomes zero, as no bending curvatures take place and/or, the bending

moments and membrane forces that are induced by thermo-electro-mechanical loading will not be involved in the clamped boundary conditions, and therefore do not appear in Eq. (55), which in these cases becomes

$$([K_0] + \lambda[K_\lambda] + \lambda_T[K_T] + [K_{\mathrm{NL}}(\Phi)])_{4NM\times 4NM}\{\Phi\}_{4NM\times 1} = \{0\}_{4NM\times 1} \tag{61}$$

This equation is solved by an iterative scheme with the following steps:

(a) Begin by solving an eigenvalue problem without considering geometric non-linearity in Eq. (61) to obtain the linear eigenvalue and corresponding eigenvector as the initial guesses of the buckling parameter and buckling mode.
(b) For a given maximum dimensionless central deflection, scale up the buckling mode and calculate the non-linear matrix $[K_{\mathrm{NL}}(\Phi)]$ to form a new eigenvalue system (61).
(c) Solve the new eigenvalue Eq. (61) to produce a new eigenvalue and eigenvector;
Repeat steps (b) and (c) until the relative difference between the eigenvalues (buckling load or buckling temperature) that is obtained from the subsequent two iterations is within the specified tolerance. Here, the error tolerance is $\eta < 10^{-3}$.
(d) Repeat step (b)–(d) to determine the postbuckling equilibrium path.
For piezoelectric FGM hybrid plates in which bending curvatures, non-uniform membrane stresses, and bending moments develop when subjected to thermo-electro-mechanical loads, the right-hand side force vector in Eq. (55) is non-zero, and eigenvalue type instability will not occur. In such a case, the modified Newton–Raphson technique will be used to obtain the equilibrium paths.

5. Results and discussion

In what follows, a symbolic notation is used to indicate the out-of-plane edge supporting condition, "CSCF": for example, when it refers to a plate that is clamped at $y = 0, 1$, simply supported at $x = 0$, and free at $x = 1$.

5.1. Convergence and comparison studies

Convergence studies are undertaken in Tables 1 and 2 by comparing the results with varying numbers of nodal lines N and truncated series number M. The present method converges well enough to yield results

Table 1
Buckling load parameter $\lambda_{\mathrm{cr}} = \bar{p}_X b^2 h/\pi^2 D$ for clamped isotropic rectangular plates that are subjected to in-plane loads

b/h	Source	Uniaxial compression		Biaxial compression	
		$a/b = 0.5$	$a/b = 1.0$	$a/b = 0.5$	$a/b = 1.0$
20	$N \times M = 9 \times 3$	9.8141	3.4245	9.4506	3.2744
	$N \times M = 13 \times 5$	17.1668	9.6251	13.3755	5.0791
	$N \times M = 17 \times 5$	17.1636	9.3884	13.3685	5.0787
	$N \times M = 21 \times 7$	17.1636	9.3867	13.3683	5.0786
	Liew et al. (2001b)	16.918	9.5227	13.766	5.0673
	Wang et al. (1993)	17.199	9.5526	13.963	5.0840
10	$N \times M = 9 \times 3$	8.2996	3.0811	7.9595	2.9973
	$N \times M = 13 \times 5$	13.2316	8.0408	10.4606	4.5736
	$N \times M = 17 \times 5$	13.2287	8.3329	10.4606	4.5734
	$N \times M = 21 \times 7$	13.2288	8.3314	10.4607	4.5734
	Liew et al. (2001b)	12.462	8.1226	10.173	4.4535
	Wang et al. (1993)	12.974	8.2733	10.541	4.5400

Table 2
Buckling temperature parameter $\lambda_{T\mathrm{cr}}$ for isotropic square plates that are subjected to uniform temperature change

Plate type	Present results				Existing results	
	$N \times M = 9 \times 3$	$N \times M = 13 \times 5$	$N \times M = 17 \times 5$	$N \times M = 21 \times 7$		
Clamped						
$b/h = 100$	0.2532	0.3333	0.3334	0.3334	0.3374[a]	0.3357[b]
Simply supported						
$b/h = 100$	0.1265	0.1265	0.1265	0.1265	0.1264[c]	0.1265[d]
$b/h = 10$	12.0018	12.0016	12.0016	12.0016	11.8300[c]	11.9778[d]
$b/h = 5$	41.6120	41.6114	41.6113	41.6113	39.90[c]	41.2971[d]

[a] Results given by Gossard et al. (1952).
[b] FSDT results given by Singha et al. (2001).
[c] HSDT results given by Shen (1998).
[d] Three-dimensional results given by Noor and Burton (1992).

with sufficient accuracy when $N \times M = 17 \times 5$ for clamped isotropic plates under uniaxial compression in Table 1, when $N \times M = 13 \times 5$ for plates that are exposed to uniform temperature change in Table 2, and for clamped isotropic plates under biaxial compression in Table 1. Hereafter, $N \times M = 17 \times 5$ is used in all numerical computations.

Before proceeding to the buckling and postbuckling analysis of piezoelectric FGM hybrid plates, four illustrative examples are solved to validate the accuracy and effectiveness of the present formulation. Direct comparisons are made between our results and those from the literature.

In Table 1, the buckling load parameter, $\lambda_{\mathrm{cr}} = \bar{p}_X b^2 h/\pi^2 D^*_{11}$, for clamped isotropic rectangular plates ($v = 0.3$) that are subjected to uniaxial and biaxial edge compression is compared to the FSDT results of Wang et al. (1993) and the 3-D solutions of Liew et al. (2001b). Good agreement is noticed.

Table 2 gives the critical temperature parameter $\lambda_{T\mathrm{cr}}$ for isotropic square plates ($v = 0.3$) that are subjected to uniform temperature change. The computation data are $b/h = 100$, 10, 5, $\alpha = 1.0 \times 10^{-6}$ for the simply supported plate, and $b/h = 100$, $\alpha = 2.0 \times 10^{-6}$ for the clamped plate. The results by Gossard et al. (1952), the 3-D elasticity solution of Noor and Burton (1992), the FSDT solution of Singha et al. (2001), and the HSDT solution of Shen (1998) are provided for comparison. Clearly, the present results agree well with these previous results.

Fig. 2 displays the postbuckling load-deflection curves for a simply supported, isotropic, moderately thick plate ($b/h = 10$, $v = 0.3$) under equal biaxial edge compression. Direct comparison shows excellent correlation between the results of the present analysis and those of Bhimaraddi (1992).

The thermal postbuckling equilibrium path for a simply supported, isotropic square plate ($v = 0.15$) under uniform temperature change is depicted in Fig. 3. The longitudinal edges of the plate are restrained: that is, the plate is immovable at $x = 0, 1$. The present curve is almost identical to that which was obtained by Librescu and Souza (1993).

5.2. Buckling of clamped FGM plates

FGM with a mixture of zirconia and aluminum for the FGM substrate and G-1195N for the piezoelectric layers is used for the plate, which is referred to as ZrO_2/Al. The actuator layer thickness is $h_a = 0.001$ m. The material properties for zirconia, aluminum, and G-1195N are listed in Table 3.

The buckling temperature parameter $\lambda_{T\mathrm{cr}} = \alpha_c \Delta T \times 10^3$ for fully immovable, clamped piezoelectric FGM hybrid rectangular plates ($a/b = 1.0$, 1.5; $a/h = 80$, 40, 20) that are subjected to uniform temperature change and constant electric field is calculated and presented in Table 4. Five electric loading cases are considered: $V_a = 0$, ± 200, ± 500 V. Here $V_a = 0$ V denotes a grounding condition. The results show that the

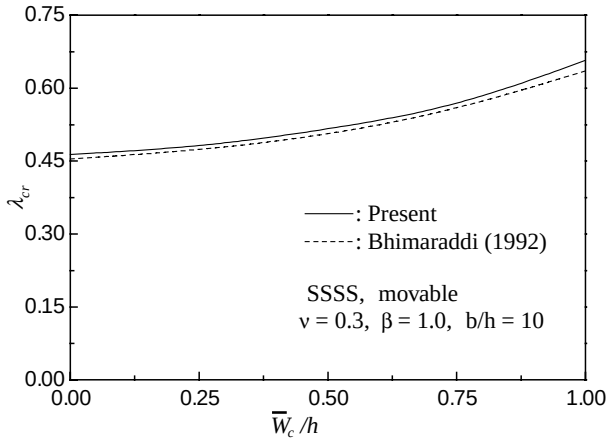

Fig. 2. Comparison of postbuckling load-deflection curves for a movable, simply supported, isotropic square plate under biaxial edge compression.

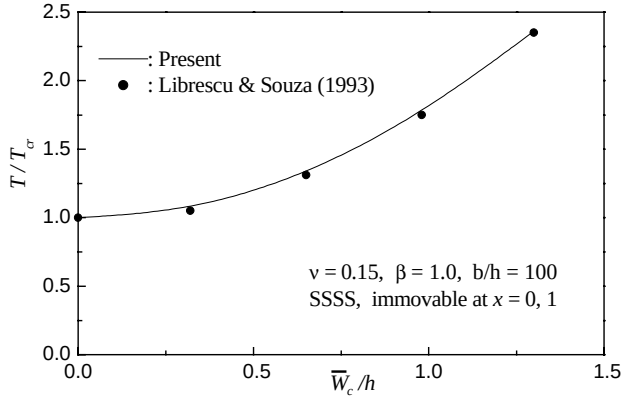

Fig. 3. Comparison of postbuckling load-deflection curves for a simply supported, isotropic square plate under uniform temperature change.

Table 3
Material properties of FGMs and piezoelectric materials

Properties	Zirconia	Aluminum	G-1195N
Elastic modulus E (GPa)	151.0	70.0	63.0
Poisson's ratio v	0.3	0.3	0.3
Coefficient of thermal expansion α (1/°C)	10^{-5}	2.3×10^{-5}	1.2×10^{-4}
Thermal conductivity κ (W/m k)	2.09	204	5.0
Piezoelectric constant d_{31} (m/V)	–	–	2.54×10^{-10}
Piezoelectric constant d_{32} (m/V)	–	–	2.54×10^{-10}

critical buckling temperature decreases with the increase of the volume fraction index n (i.e., as the amount of zirconia reduces), and increases as the plate aspect ratio a/b becomes larger. Moreover, the buckling temperature can be increased by applying negative voltage on the actuator layers, because it makes the plate

Table 4
Buckling temperature rise (°C) for fully immovable, clamped piezoelectric FGM hybrid rectangular plates that are subjected to uniform temperature change and a constant electric field

Actuator voltage V_a (V)	$a/b = 1.0$					$a/b = 1.5$				
	ZrO_2	$n = 0.2$	$n = 2.0$	$n = 5.0$	Al	ZrO_2	$n = 0.2$	$n = 2.0$	$n = 5.0$	Al
$a/h = 80$										
500	22.744	15.258	9.5772	8.7394	4.5573	51.153	37.226	26.785	25.646	18.686
200	29.102	21.137	15.171	14.515	10.521	55.392	41.145	30.514	29.497	22.662
0	33.341	25.056	18.899	18.365	14.496	58.218	43.758	33.000	32.063	25.312
−200	37.580	28.976	22.628	22.216	18.472	61.044	46.371	35.486	34.630	27.963
−500	43.939	34.855	28.222	27.991	24.435	65.283	50.290	39.215	38.481	31.938
$a/h = 40$										
500	190.78	140.73	103.15	99.281	74.949	351.64	263.41	197.07	190.78	149.33
200	200.31	149.55	111.54	107.94	83.894	355.88	267.33	200.80	194.63	153.31
0	206.70	155.43	117.14	113.72	89.857	358.71	269.94	203.29	197.20	155.96
−200	213.03	161.31	122.73	119.50	95.821	361.53	272.56	205.78	199.77	158.61
−500	222.57	170.13	131.12	128.16	104.77	365.77	276.47	209.50	203.62	162.59
$a/h = 20$										
500	787.42	590.93	441.15	426.02	334.36	1359.1	1025.8	767.57	740.25	587.37
200	796.96	599.75	449.54	434.68	343.30	1363.4	1029.7	771.30	744.10	591.34
0	803.32	605.63	455.13	440.50	349.27	1366.2	1032.3	773.79	746.68	593.99
−200	809.67	611.51	460.72	446.23	355.23	1369.0	1034.9	776.27	749.24	596.64
−500	819.21	620.33	469.11	454.98	364.18	1373.3	1038.8	780.00	753.09	600.62

contract. In contrast, positive voltage makes the plate stretch, and accordingly decreases the buckling temperature.

Table 5 compares the buckling load parameter $\lambda_{cr} = \bar{p}_X b^2/(\pi^2 D_0)$ for clamped piezoelectric FGM hybrid rectangular plates ($a/b = 1.0, 2.0, 4.0$; $a/h = 100, 40, 20, 10$) that are movable at all edges and subjected to uniaxial and biaxial edge compression. D_0 is chosen to be the value of D_{11}^* of an isotropic zirconia plate with $a/h = 10$. The buckling load is dramatically reduced as a/b changes from 1.0 to 4.0. It is noteworthy that for a fully movable plate, the constant actuator voltage has no effect on the critical buckling load because the electrically induced deformation can develop freely in the in-plane direction of the plate.

The buckling problem of initially stressed clamped piezoelectric FGM hybrid plates under combined loads is also studied. Critical buckling load parameter λ_{cr} is given in Table 6 for thermally prestressed square plates that are movable at $x = 0, 1$ and subjected to uniaxial compression in the x-axis while under constant actuator voltage $V_a = \pm 200$ V. The plates are assumed to be initially loaded by various uniform temperature change: $\mu = 0.0, 0.2, 0.4, 0.6$, where $\mu = \Delta T/\Delta T_{cr}^0$ is the thermal load factor and ΔT_{cr}^0 refers to the critical value of the temperature change for the plates without mechanical and electric loads. As expected, the buckling load decreases as the temperature increases.

In Tables 4 and 6, the effect of actuator voltage becomes more obvious as the side-to-thickness ratio a/h increases, and appears to be rather slight in the case of $a/h = 10$. This indicates that applied voltage in the piezoelectric actuator layers will play a more important role in controlling the bifurcation buckling in thinner FGM plates.

5.3. Thermo-electro-mechanical postbuckling of FGM plates

This section describes the postbuckling analysis of piezoelectric FGM hybrid plates under thermo-electro-mechanical loads. The results are given in dimensionless form in Figs. 4–9, in terms of the

Table 5
Buckling load parameter λ_{cr} for movable, clamped piezoelectric FGM hybrid rectangular plates that are subjected to uniform edge compression

Material composition	Uniaxial compression			Biaxial compression		
	$a/b = 1.0$	$a/b = 2.0$	$a/b = 4.0$	$a/b = 1.0$	$a/b = 2.0$	$a/b = 4.0$
$a/h = 100$						
ZrO_2	9.7809	6.5255	3.3300	5.2700	3.8918	2.7899
$n = 0.2$	7.9366	5.1951	2.6662	4.2634	3.1647	2.2373
$n = 2.0$	6.3089	4.3974	2.2179	3.3958	2.5074	1.8488
$n = 5.0$	5.9428	4.0738	2.0608	3.1958	2.3587	1.7223
Aluminum	4.5342	3.0251	1.5437	2.4430	1.8041	1.2933
$a/h = 40$						
ZrO_2	9.6938	5.6245	2.7629	5.2267	3.8001	2.3661
$n = 0.2$	7.8723	4.4824	2.2241	4.2514	3.0965	1.9088
$n = 2.0$	6.2517	3.7926	1.8414	3.3676	2.4476	1.5691
$n = 5.0$	5.8829	3.5047	1.6972	3.1662	2.2964	1.4487
Aluminum	4.4938	2.6074	1.2808	2.4230	1.7617	1.0969
$a/h = 20$						
ZrO_2	9.3922	4.6125	2.0500	5.0789	3.5072	1.7627
$n = 0.2$	7.6484	3.7346	1.6790	4.1413	2.8762	1.4480
$n = 2.0$	6.0544	3.0833	1.3594	3.2711	2.2568	1.1635
$n = 5.0$	5.6770	2.8074	1.2291	3.0658	2.0998	1.0522
Aluminum	4.3540	2.1383	0.9504	2.3545	1.6258	0.8171
$a/h = 10$						
ZrO_2	8.3229	2.8570	1.1441	4.5734	2.7013	0.9640
$n = 0.2$	6.8602	2.3795	0.9595	3.7599	2.2573	0.8116
$n = 2.0$	5.3683	1.8829	0.7514	2.9421	1.7304	0.6309
$n = 5.0$	4.9717	1.6758	0.6655	2.7287	1.5761	0.5578
Aluminum	3.8673	1.3245	0.5304	2.1201	1.2522	0.4469

dimensionless load parameter $\lambda_x = \bar{p}_X b^2/(4\pi^2 D_0)$ or the temperature parameter $\lambda_T = \alpha_c \Delta T \times 10^3$ against the dimensionless central deflection $\overline{W}_c/h$.

Fig. 4 shows the compressive postbuckling response of fully movable, clamped piezoelectric FGM hybrid square plates ($a/h = 10$) under equal biaxial edge compression. As expected, the postbuckling load-carrying capacity is the maximum for the isotropic zirconia plate, the minimum for the isotropic aluminum plate, and decreases as the volume fraction index n increases due to the degradation in the plate stiffness. This trend can also be observed in the other examples. Clamped piezoelectric FGM hybrid plates do exhibit bifurcation-type instability, and the bifurcation point is represented by the intersection of the postbuckling curve with the load ordinate, and corresponds to the critical buckling load. In these cases, the prebuckling path overlaps the load ordinate. Note that the postbuckling curve for the plate with $n = 0.2$ suddenly goes down when $\overline{W}_c/h > 0.9$.

Fig. 5 gives the postbuckling response for movable CSCS and CSCF piezoelectric FGM hybrid square plates under the same loading condition. Compared with CSCS plates, the CSCF plates are capable of carrying higher loads in the postbuckling phase. The results also confirm that when the plate is neither isotropic nor fully clamped, bifurcation-type instability cannot take place. Irrespective of the magnitude of in-plane forces or temperature change, the existence of bending–stretching couplings in these graded plates not only gives rise to bending moments and in-plane stresses, but also produces lateral deflections, as was discussed in Section 4.2.1.

Moreover, the postbuckling curve for CSCS plates with $n = 0.2$ suddenly drops at about $\overline{W}_c/h > 0.44$ and then steadily increases, which indicates the possibility of the occurrence of secondary instability: that is,

Table 6
Buckling load parameter λ_{cr} for thermally prestressed, clamped piezoelectric FGM hybrid square plates that are movable at $x = 0, 1$ and subjected to uniaxial compression and a constant electric field

Temperature rise, μ	$V_a = -200$ V					$V_a = 200$ V				
	ZrO_2	$n = 0.2$	$n = 2.0$	$n = 5.0$	Al	ZrO_2	$n = 0.2$	$n = 2.0$	$n = 5.0$	Al
$a/h = 100$										
0.0	5.6127	4.6247	3.7383	3.5387	2.7840	4.9238	3.9380	3.0481	2.8473	2.0946
0.2	4.6778	3.8897	3.0990	2.9214	2.3183	4.1107	3.3245	2.5306	2.3522	1.7505
0.4	3.7110	3.1299	2.4383	2.2837	1.8373	3.2661	2.6839	1.9935	1.8393	1.3916
0.6	2.6847	2.3142	1.7419	1.6140	1.3292	2.3585	1.9714	1.4210	1.2968	1.0023
$a/h = 40$										
0.0	5.2818	4.3063	3.4228	3.2215	2.4780	5.1715	4.1963	3.3122	3.1108	2.3677
0.2	4.4018	3.6245	2.8373	2.6588	2.0649	4.3109	3.5340	2.7462	2.5676	1.9740
0.4	3.4898	2.9171	2.2312	2.0766	1.6369	3.4185	2.8456	2.1599	2.0054	1.5655
0.6	2.5175	2.1487	1.5897	1.4637	1.1810	2.4653	2.0940	1.5384	1.4129	1.1288
$a/h = 20$										
0.0	5.0928	4.1551	3.2850	3.0979	2.3683	5.0651	4.1275	3.2572	3.0519	2.3406
0.2	4.2340	3.4885	2.7176	2.5373	1.9689	4.2111	3.4658	2.6947	2.5144	1.9460
0.4	3.3419	2.7948	2.1288	1.9749	1.5540	3.3239	2.7768	2.1109	1.9570	1.5361
0.6	2.3913	2.0422	1.5058	1.3829	1.1120	2.3782	2.0286	1.4929	1.3701	1.0990
$a/h = 10$										
0.0	4.5770	3.7634	2.9456	2.7322	2.1237	4.5700	3.7564	2.9386	2.7252	2.1167
0.2	3.7766	3.1295	2.4230	2.2421	1.7523	3.7708	3.1237	2.4172	2.2362	1.7465
0.4	2.9407	2.4660	1.8781	1.7312	1.3645	2.9362	2.4614	1.8735	1.7266	1.3599
0.6	2.0549	1.7545	1.3032	1.1941	0.9535	2.0516	1.7512	1.2999	1.1909	0.9502

a snap-through phenomenon may take place. Generally, the transition from the primary postbuckling path to the secondary postbuckling path is associated with the change of the postbuckling displacement mode shape.

Fig. 6 investigates the thermally induced postbuckling behavior of fully immovable, clamped piezoelectric FGM hybrid square plates with side-to-thickness $a/h = 20$ under uniform temperature change. The effect of the actuator voltage is also examined. The solid lines and the dashed lines represent the postbuckling response for the cases of $V_a = -200$ and 200 V respectively. As revealed in our buckling analysis, the application of negative voltage does improve the postbuckling strength to some extent, though not significantly. It is interesting to see that in the large deflection stage, the graded plate with $n = 5.0$ gains postbuckling strength marginally, while other plates can develop greater load-carrying capacity.

Thermo-electro-mechanical postbuckling analysis is performed in Figs. 7–9 for clamped piezoelectric FGM hybrid square plates that are immovable at $y = 0, 1$ but movable at $x = 0, 1$. Parametric studies are undertaken to highlight the influence of in-plane prestress, prescribed temperature change, and the side-to-thickness ratio on the postbuckling characteristics. The postbuckling paths under the combined action of temperature change, applied voltage, and mechanical loads are somewhat different from those which are obtained in mechanically or thermally induced postbuckling problems.

In Fig. 7, we assume that the plate ($a/h = 10$) is subjected to edge compression on the x-axis and is undergoing a uniform temperature change ΔT ($= 100$, 300 °C). The applied actuator voltage is fixed at $V_a = -200$ V. All graded plates in this example will experience secondary instability. It is also evident from the figure that, in general, the higher the temperature, the lower is the postbuckling strength. However, this does not hold for piezoelectric FGM hybrid plates with $n = 0.2$ and 2. In these two cases, postbuckling paths at $\Delta T = 300$ °C surpass those at $\Delta T = 100$ °C when $\overline{W}_c/h > 0.4$.

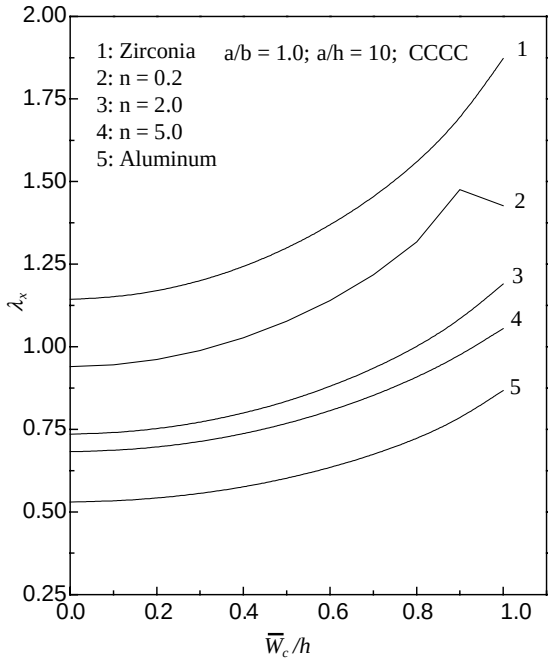

Fig. 4. Postbuckling response of movable, clamped hybrid square plates under equal biaxial compression.

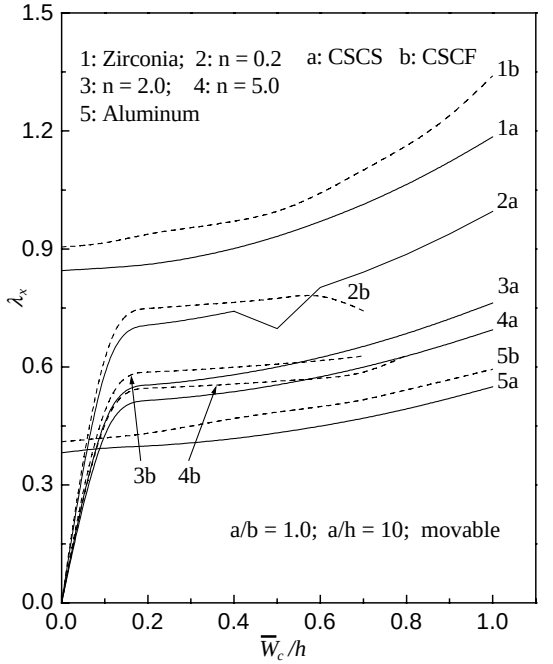

Fig. 5. Postbuckling response of movable, CSCS and CSCF hybrid square plates subjected to equal biaxial compression.

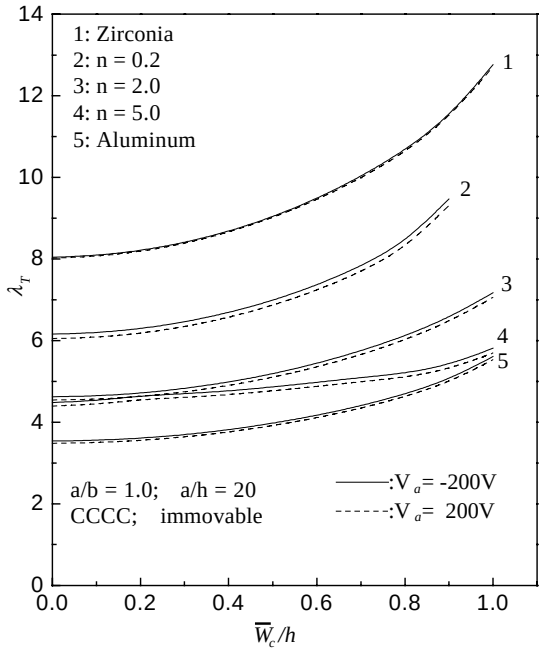

Fig. 6. Thermal postbuckling response of immovable, clamped hybrid square plates under uniform temperature rise and at constant actuator voltage.

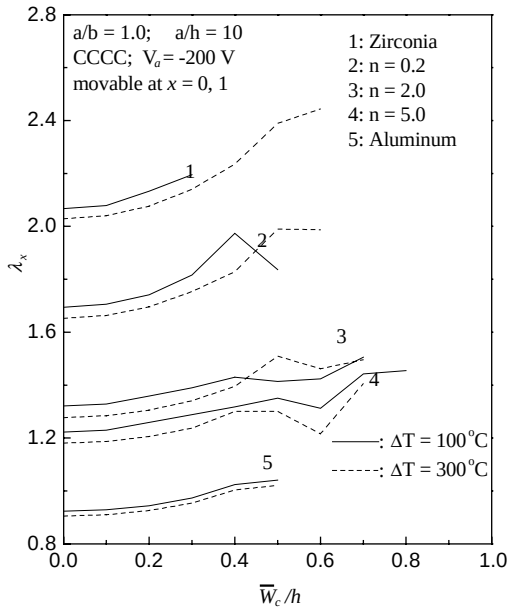

Fig. 7. Effect of temperature rise on thermo-electro-mechanical postbuckling response of clamped hybrid square plates under uniaxial compression and constant actuator voltage.

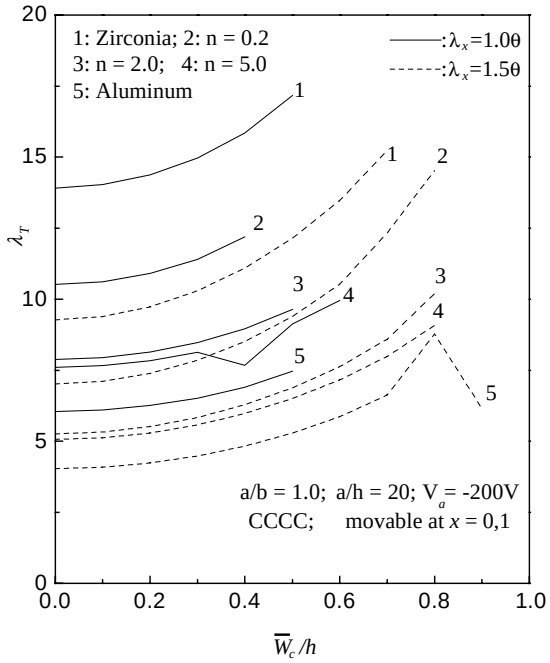

Fig. 8. Effect of edge compression on thermo-electro-mechanical postbuckling response of clamped hybrid square plates subjected to uniform temperature rise and constant actuator voltage.

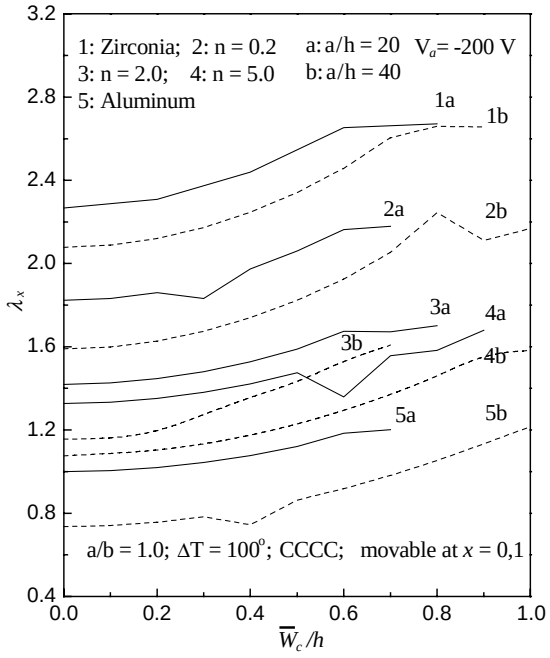

Fig. 9. Effect of side-to-thickness ratio on thermo-electro-mechanical postbuckling of clamped hybrid square plates.

The effect of the in-plane load on the non-linear relationship of postbuckling temperature versus central deflection is displayed in Fig. 8 for piezoelectric FGM hybrid plates ($a/h = 20$) that are subjected to a given edge compression on the x-axis, a constant electric load $V_a = -200$ V, and uniform temperature change. The solid lines and dashed lines are for the cases of $\lambda_x = 1.0\theta$ and $\lambda_x = 1.5\theta$ respectively, where $\theta = (D_{11}^* D_{22}^*)^{1/2}/D_0$. The postbuckling resistance decreases considerably with the increase in the compressive edge load.

Fig. 9 depicts the thermo-electro-mechanical postbuckling behavior of piezoelectric FGM hybrid square plates with side-to-thickness ratio $a/h = 20$, 40. The plates are subjected to uniaxial compression on the x-axis, a temperature change $\Delta T = 100$ °C, and a constant actuator voltage $V_a = -200$ V. The solid lines and the dashed lines are for $a/h = 20$, 40 respectively. It is evident from the results that the postbuckling paths for thicker piezoelectric FGM hybrid plates are higher than for thinner ones. It appears that secondary instability sets in at relatively small deflections in the cases of the purely aluminum plate of $a/h = 40$ and the graded plate of $a/h = 20$ and $n = 0.2$.

As shown in Figs. 4–9, many postbuckling paths cannot be traced beyond certain load values because of convergence problems in the iteration process. This phenomenon may be attributable to the fact that the expected deformation beyond these loads could not be obtained by the iterative process.

6. Conclusions

This paper investigates the postbuckling response of piezoelectric FGM hybrid rectangular plates under the combined action of uniform temperature change, edge compression, and a constant applied actuator voltage based on Reddy's HSDT. A semi-analytical DQ-based iteration technique is used to determine the thermo-electro-mechanical postbuckling response for plates with two opposite clamped edges. Postbuckling equilibrium paths are presented for ZrO_2/Al rectangular plates in terms of the postbuckling load/temperature parameter versus central deflection. Dimensionless critical buckling load and temperature parameters are given in tabular form for clamped hybrid plates. Our results indicate that for hybrid plates which are not fully clamped, wherein bending curvatures appear from the commencement of loading, bifurcation buckling does not exist due to the bending–stretching coupling effect. Furthermore, secondary instability occurs in the thermo-electro-mechanical postbuckling equilibrium paths in many cases. The application of negative voltage in the actuator layers can improve the buckling and postbuckling strength, but this effect tends to be weaker as the side-to-thickness ratio a/h decreases, and seems to be very slight when a/h reaches 10. The effects of material composition, temperature change, in-plane forces, and boundary conditions on the buckling and postbuckling behavior of hybrid plates are discussed and demonstrated through illustrative numerical examples.

Acknowledgements

The work described in this paper was supported by grants from the Research Council of the Hong Kong Special Administrative Region [project nos. CityU 1024/01E and CityU 1036/01E] and the Australian Research Council (A00104534).

Appendix A

Dimensionless quantities of γ_{ij} and γ_{ijk} are given as follows:

$$\gamma_{14} = [D_{22}^*/D_{11}^*]^{1/2}, \quad \gamma_{24} = [A_{11}^*/A_{22}^*]^{1/2}, \quad \gamma_5 = -A_{12}^*/A_{22}^*$$

$$(\gamma_{110},\gamma_{112},\gamma_{114}) = c_1[F_{11}^*,(F_{12}^*+F_{21}^*+4F_{66}^*)/2,F_{22}^*]/D_{11}^*$$

$$(\gamma_{120},\gamma_{122}) = [(D_{11}^*-c_1F_{11}^*),(D_{12}^*-c_1F_{12}^*+2D_{66}^*-2c_1F_{66}^*)]/D_{11}^*$$

$$(\gamma_{131},\gamma_{133}) = [(D_{12}^*-c_1F_{21}^*+2D_{66}^*-2c_1F_{66}^*),(D_{22}^*-c_1F_{22}^*)]/D_{11}^*$$

$$(\gamma_{140},\gamma_{142},\gamma_{144}) = [B_{21}^*,(B_{11}^*+B_{22}^*-2B_{66}^*),B_{12}^*]/\Delta$$

$$(\gamma_{212},\gamma_{612}) = [(2A_{12}^*+A_{66}^*)/2,A_{12}^*]/A_{22}^*$$

$$(\gamma_{220},\gamma_{222}) = [(B_{21}^*-c_1E_{21}^*),B_{11}^*-B_{66}^*-c_1(E_{11}^*-E_{66}^*)]/\Delta$$

$$(\gamma_{231},\gamma_{233}) = [B_{22}^*-B_{66}^*-c_1(E_{22}^*-E_{66}^*),(B_{12}^*-c_1E_{12}^*)]/\Delta$$

$$(\gamma_{240},\gamma_{242},\gamma_{244}) = c_1[E_{21}^*,(E_{11}^*+E_{22}^*-2E_{66}^*),E_{12}^*]/\Delta$$

$$(\gamma_{310},\gamma_{312}) = c_1[(F_{11}^*-c_1H_{11}^*),(F_{21}^*+2F_{66}^*-c_1(H_{12}^*+2H_{66}^*))]/D_{11}^*$$

$$(\gamma_{320},\gamma_{322},\gamma_{331}) = [(D_{11}^*-2c_1F_{11}^*+c_1^2H_{11}^*),(D_{66}^*-2c_1F_{66}^*+c_1^2H_{66}^*),D_{12}^*+D_{66}^* - c_1(F_{12}^*+F_{21}^*+2F_{66}^*)+c_1^2(H_{12}^*+H_{66}^*)]/D_{11}^*$$

$$(\gamma_{411},\gamma_{413}) = c_1[F_{12}^*+2F_{66}^*-c_1(H_{12}^*+2H_{66}^*),F_{22}^*-c_1H_{22}^*]/D_{11}^*$$

$$(\gamma_{430},\gamma_{432}) = [(D_{66}^*-2c_1F_{66}^*+c_1^2H_{66}^*),(D_{22}^*-2c_1F_{22}^*+c_1^2H_{22}^*)]/D_{11}^*$$

$$(\gamma_{31},\gamma_{41}) = [(A_{55}^*-6c_1D_{55}^*+9c_1^2F_{55}^*),(A_{44}^*-6c_1D_{44}^*+9c_1^2F_{44}^*)]/D_{11}^*$$

$$(\gamma_{511},\gamma_{512},\gamma_{516},\gamma_{517},\gamma_{518}) = [B_{11}^*-c_1E_{11}^*,B_{21}^*-c_1E_{21}^*,B_{66}^*-c_1E_{66}^*,B_{12}^*-c_1E_{12}^*,B_{22}^*-c_1E_{22}^*]/\Delta$$

$$(\gamma_{611},\gamma_{612},\gamma_{633}) = [A_{11}^*,A_{12}^*,A_{66}^*]/A_{22}^*$$

$$(\gamma_{711},\gamma_{712},\gamma_{721},\gamma_{722},\gamma_{733}) = [B_{11}^*,B_{12}^*,B_{21}^*,B_{22}^*,B_{66}^*]/\Delta$$

$$(\gamma_{M10},\gamma_{M12},\gamma_{M13},\gamma_{M14}) = [(D_{11}^*-c_1F_{11}^*),(D_{21}^*-c_1F_{21}^*),c_1F_{11}^*,c_1F_{21}^*]/D_{11}^*$$

$$(\gamma_{M20},\gamma_{M22},\gamma_{M23},\gamma_{M24}) = [(D_{12}^*-c_1F_{12}^*),(D_{22}^*-c_1F_{22}^*),c_1F_{12}^*,c_1F_{22}^*]/D_{11}^*$$

$$(\gamma_{M31},\gamma_{M35},\gamma_{p31},\gamma_{p35}) = [(D_{66}^*-c_1F_{66}^*),c_1F_{66}^*,c_1(F_{66}^*-c_1H_{66}^*),c_1^2H_{66}^*]/D_{11}^*$$

$$(\gamma_{p10},\gamma_{p12},\gamma_{p13},\gamma_{p14}) = c_1[(F_{11}^*-c_1H_{11}^*),(F_{12}^*-c_1H_{12}^*),c_1H_{11}^*,c_1H_{12}^*]/D_{11}^*$$

$$(\gamma_{p20},\gamma_{p22},\gamma_{p23},\gamma_{p24}) = c_1[(F_{21}^*-c_1H_{21}^*),(F_{22}^*-c_1H_{22}^*),c_1H_{21}^*,c_1H_{22}^*]/D_{11}^*$$

$$(\gamma_{p16},\gamma_{p18},\gamma_{p26},\gamma_{p28},\gamma_{p37}) = c_1[E_{21}^*,E_{11}^*,E_{22}^*,E_{12}^*,E_{66}^*]/\Delta$$

$$(\gamma_{m11},\gamma_{m21},\gamma_{m31}) = [2c_1(c_1H_{66}^*-F_{66}^*)/D_{11}^*,(B_{66}^*-c_1E_{66}^*)/\Delta,(D_{66}^*+c_1^2H_{66}^*-2c_1F_{66}^*)/D_{11}^*]$$

$$(\gamma_{Q10},\gamma_{Q12},\gamma_{Q20},\gamma_{Q22}) = c_1[c_1H_{11}^*/D_{11}^*,c_1(4H_{66}^*+H_{12}^*)/D_{11}^*,E_{21}^*/\Delta,(2E_{66}^*-E_{11}^*)/\Delta]$$

$$(\gamma_{Q30},\gamma_{Q32},\gamma_{Q34}) = c_1[(F_{11}^* - c_1H_{11}^*), 2(F_{66}^* - c_1H_{66}^*), (F_{12}^* + 2F_{66}^* - c_1H_{12}^* - 2c_1H_{66}^*)]/D_{11}^*$$

$$(\gamma_{T1},\gamma_{T2}) = (A_X^{\mathrm{T}}, A_Y^{\mathrm{T}})a^2/1000\alpha_{\mathrm{c}}(D_{11}^*D_{22}^*)^{1/2}, \quad (\gamma_{T4},\gamma_{T5},\gamma_{T7},\gamma_{T8}) = (D_X^{\mathrm{T}}, D_Y^{\mathrm{T}}, F_X^{\mathrm{T}}, F_Y^{\mathrm{T}})a^2/1000\alpha_{\mathrm{c}}\Delta D_{11}^*$$

$$(\gamma_{E1},\gamma_{E2}) = (A_X^{\mathrm{E}}, A_Y^{\mathrm{E}})a^2/(D_{11}^*D_{22}^*)^{1/2}, \quad (\gamma_{E4},\gamma_{E5},\gamma_{E7},\gamma_{E8}) = (D_X^{\mathrm{E}}, D_Y^{\mathrm{E}}, F_X^{\mathrm{E}}, F_Y^{\mathrm{E}})a^2/\Delta D_{11}^*$$

References

Bert, C.W., Malik, M., 1996. Differential quadrature method in computational mechanics: a review. Applied Mechanics Review 49, 1–28.

Bhimaraddi, A., 1992. Buckling and postbuckling behavior of laminated plates using the generalized nonlinear formulation. International Journal of Mechanical Sciences 34, 703–715.

Chee, C.Y.K., Tong, L.Y., Steven, G.P., 1998. A review on the modelling of piezoelectric sensors and actuators incorporated in intelligent structures. Journal of Intelligent Material Systems and Structures 9, 3–19.

Feldman, E., Aboudi, J., 1997. Buckling analysis of functionally graded plates subjected to uniaxial loading. Composite Structures 38, 29–36.

Gossard, M.L., Seide, P., Roberts, W.M., 1952. Thermal buckling of plates. NACA TND, USA. p. 2771.

He, X.Q., Ng, T.Y., Sivashanker, S., Liew, K.M., 2001. Active control of FGM plates with integrated piezoelectric sensors and actuators. International Journal of Solids and Structures 38, 1641–1655.

He, X.Q., Liew, K.M., Ng, T.Y., Sivashanker, S., 2002. A FEM model for the active control of curved FGM shells using piezoelectric sensor/actuator layers. International Journal for Numerical Methods in Engineering 54, 853–870.

Irschik, H., 2002. A review on static and dynamic shape control of structures by piezoelectric actuation. Engineering Structures 24, 5–11.

Leissa, A.W., 1986. Conditions for laminated plates to remain flat under in-plane loading. Composite Structures 6, 261–270.

Librescu, L., Souza, M.A., 1993. Post-buckling of geometrically imperfect shear-deformable flat panels under combined thermal and compressive edge loadings. ASME, Journal of Applied Mechanics 60, 526–533.

Liew, K.M., Liang, J., 2002. Modeling of 3D transversely piezoelectric and elastic bimaterials using the boundary element method. Computational Mechanics 29, 151–162.

Liew, K.M., Han, J.B., Xiao, Z.M., 1996. Differential quadrature method for thick symmetric cross-ply laminates with first-order shear flexibility. International Journal of Solids and Structures 38, 2647–2658.

Liew, K.M., He, X.Q., Ng, T.Y., Sivashanker, S., 2001a. Active control of FGM plates subjected to a temperature gradient: modelling via finite element method based on FSDT. International Journal for Numerical Methods in Engineering 52, 1253–1271.

Liew, K.M., Teo, T.M., Han, J.B., 2001b. Three-dimensional static solutions of rectangular plates by variant differential quadrature method. International Journal of Mechanical Sciences 43, 1611–1628.

Liew, K.M., He, X.Q., Ng, T.Y., Kitipornchai, S., 2002. Active control of FGM shells subjected to a temperature gradient via piezoelectric sensor/actuator patches. International Journal for Numerical Methods in Engineering 55, 653–668.

Ng, T.Y., Lam, K.Y., He, X.Q., Liew, K.M., 2002. Finite element modeling of active control of functionally graded shells in frequency domain via piezoelectric sensors and actuators. Computational Mechanics 28, 1–9.

Noor, A.K., Burton, W.S., 1992. Three-dimensional solutions for the thermal buckling of multilayered anisotropic plates. Journal of Engineering Mechanics ASCE 118, 683–701.

Oh, I.K., Han, J.H., Lee, I., 2000. Postbuckling and vibration characteristics of piezolaminated composite plate subject to thermo-piezoelectric loads. Journal of Sound and Vibration 233, 19–40.

Ootao, Y., Tanigawa, Y., 2000. Three-dimensional transient piezothermoelasticity in functionally graded rectangular plate bonded to a piezoelectric plate. International Journal of Solids and Structures 37, 4377–4401.

Qatu, M.S., Leissa, A.W., 1993. Buckling or transverse deflections of unsymmetrically laminated plates subjected to in-plane loads. AIAA Journal 31, 189–194.

Praveen, G.N., Reddy, J.N., 1998. Nonlinear transient thermoelastic analysis of functionally graded ceramic-metal plates. International Journal of Solids and Structures 35, 4457–4476.

Reddy, J.N., 1984. A refined nonlinear theory of plates with transverse shear deformation. International Journal of Solids and Structures 20, 881–896.

Reddy, J.N., 2000. Analysis of functionally graded plates. International Journal for Numerical Methods in Engineering 47, 663–684.

Shen, H.S., 1998. Thermal postbuckling analysis of imperfect Reissner–Mindlin plates on softening nonlinear elastic foundations. Journal of Engineering Mathematics 33, 259–270.

Shen, H.S., 2001a. Thermal postbuckling analysis of shear-deformable laminated plates with piezoelectric actuators. Composites Science and Technology 61, 1931–1943.

Shen, H.S., 2001b. Postbuckling of shear deformable laminated plates with piezoelectric actuators under complex loading conditions. International Journal of Solids and Structures 38, 7703–7721.

Shen, H.S., 2002. Nonlinear bending response of functionally graded plates subjected to transverse loads and in thermal environments. International Journal of Mechanical Sciences 44, 561–584.

Singha, M.K., Ramachandra, L.S., Bandyopadhyay, J.N., 2001. Thermal postbuckling analysis of laminated composite plates. Composite Structures 54, 453–458.

Tanigawa, Y., Ootao, Y., Kawamura, R., 1991. Thermal bending of laminated composite rectangular plates and nonhomogeneous plates due to partial heating. Journal of Thermal Stresses 14, 285–308.

Wang, C.M., Liew, K.M., Xiang, Y., Kitipornchai, S., 1993. Buckling of rectangular Mindlin plates with internal supports. International Journal of Solids and Structures 30, 1–17.

Yang, J., Shen, H.S., 2002a. Vibration characteristics and transient response of shear deformable functionally graded plates in thermal environment. Journal of Sound and Vibration 255, 579–602.

Yang, J., Shen, H.S., 2002b. Nonlinear analysis of functionally graded plates under transverse and in-plane loads. International Journal of Non-Linear Mechanics 38, 467–482.